

pubs.acs.org/JPCB Article

# Role of Cholesterol on Binding of Amyloid Fibrils to Lipid Bilayers

Cristiano L. Dias,\* Sharareh Jalali, Yanxing Yang, and Luis Cruz



Cite This: J. Phys. Chem. B 2020, 124, 3036-3042



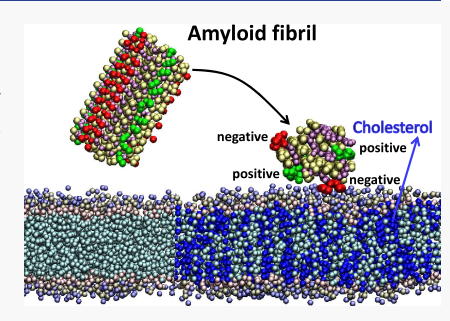
**ACCESS** 

Metrics & More



Supporting Information

**ABSTRACT:** Molecular dynamics simulations are used to provide insights into the molecular mechanisms accounting for binding of amyloid fibrils to lipid bilayers and to study the effect of cholesterol in this process. We show that electrostatic interactions play an important role in fibril—bilayer binding and cholesterol modulates this interaction. In particular, the interaction between positive residues and lipid head groups becomes more favorable in the presence of cholesterol. Consistent with experiments, we find that cholesterol enhances fibril—membrane binding.



# **■ INTRODUCTION**

Alzheimer's disease (AD) is believed to emerge from the aggregation of amyloid- $\beta$  (A $\beta$ ) proteins into soluble oligomers and fibril deposits. 1-3 Small oligomeric species can target specific membrane receptors and/or the plasma membrane in a nonspecific manner. 4,5 Amyloid fibrils have been shown to interact with lipid bilayers altering their structure and causing membrane depolarization.<sup>6–8</sup> The lipid content of bilayers can play a critical role in these processes affecting AD. 9-14 Accordingly, increased cholesterol levels at midlife strongly correlate with A $\beta$  deposition and the risk of developing AD later in life. 15-18 This lipid, which is an important component of the neuron plasma membrane, <sup>19</sup> has been shown to affect production, <sup>20–22</sup> aggregation rate, <sup>23,24</sup> and absorption <sup>25,26</sup> of  $A\beta$  proteins into bilayers. Although critical to understand AD, the molecular mechanisms accounting for the role of cholesterol in these processes remain to be fully understood. Here, we propose a molecular mechanism to explain the effects of cholesterol on the binding of  $A\beta$  fibrils to bilayers.

Cytotoxicity of amyloid fibrils is usually described in terms of their effects on cell membranes. These effects include amyloid fibrils piercing the cell membrane (perforation effect), 29,30 absorbing lipids from the bilayer (detergent effect), and/or being deposited onto one of the membrane leaflets (carpeting effect). These effects cause membrane deformation and leakage of molecules from inside small vesicles. The preference for one of these effects over the others at a specific condition is expected to depend on the geometry/structure of the amyloid fibril, activature of the lipid bilayer, and the type/strength of fibril—lipid interactions. Electrostatic interactions were shown to play an important role in fibril—membrane binding, wherein bilayers containing anionic lipids promote anchorage of fibrils into the bilayer surface. Another important lipid affecting fibril—membrane binding is cholesterol. Atomic force microscopy

showed that fibril absorption into zwitterionic membrane surfaces (carpeting effect) increases with cholesterol content. This is consistent with the cholesterol's effect of promoting the incorporation of soluble amyloid proteins into the bilayer, which has been related to the formation of amyloid pores. These effects of cholesterol appear counterintuitive as this lipid is located deep inside bilayers without significant access to proteins in the solvents. Moreover, cholesterol is mostly nonpolar and, thus, it cannot contribute directly to the electrostatic anchorage of fibrils to bilayer. In membranes with more complex lipid composition, cholesterol is involved in lipid raft formation, which can affect fibril—membrane interactions. 41–43

Computer simulations have provided additional confirmation that, for zwitterionic bilayers, fibril—membrane binding is dominated by electrostatic as opposed to van der Waals interactions. A4,45 Moreover, simulations have provided insights into fibril—membrane conformations along proposed pathways of fibril insertion. For monomeric  $A\beta$ , all-atom simulations have shown that electrostatic interactions provide the initial driving force for absorption followed by hydrophobic interactions between nonpolar residues and the bilayer. In this process, negatively charged residues of  $A\beta$  and phosphate groups can interact via  $Ca^{2+}$  ionic bridges. A5,47 In one study, increased cholesterol levels promoted the binding of monomeric  $A\beta_{1-42}$  to bilayers. This was rationalized in terms of changes in the physicochemical properties of the bilayer upon cholesterol addition, including increased surface

Received: January 17, 2020 Revised: March 20, 2020 Published: March 24, 2020





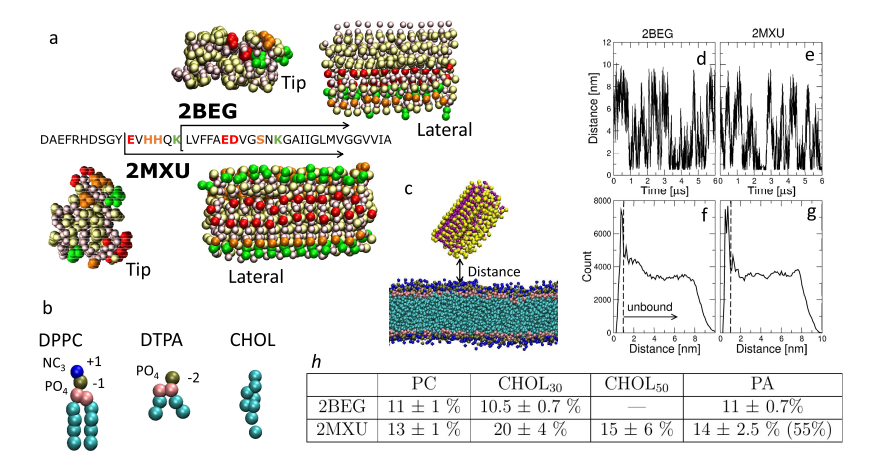


Figure 1. (a) Amino acid sequence and structure of 2BEG and 2MXU fibrils. Positive, negative, polar, and nonpolar side chains are shown in green, red, orange, and yellow, respectively. Backbone beads are shown in pink. (b) Martini representation of the different lipids used in this work, as well as the charges of their head groups. (c) Schematic representation of the minimal distance between the fibril and PO<sub>4</sub> atoms of DPPC lipids. Minimal distances of (d) 2BEG and (e) 2MXU fibrils to DPPC lipid bilayers in 6  $\mu$ s trajectories. Histogram of minimal distances to PC bilayers computed from four trajectories of (f) 2BEG and (g) 2MXU fibrils. The cutoff distance of 1 nm used to distinguish between bound and unbound states is shown as dashed vertical lines. (h) Percentage of time 2BEG and 2MXU fibrils are bound to different lipid bilayers. Trajectories with irreversible fibril—membrane binding are reported in parentheses for the PA system. Simulations of 2BEG fibril with CHOL<sub>50</sub> bilayers were not performed due to the lack of sensitivity of this fibril to lipid composition. Errors were estimated using block average, wherein trajectories were divided into blocks spanning 1.5  $\mu$ s in time.

hydrophobicity, altered lipid-ordered packing, and reduced lipid mobility. In another all-atom replica-exchange molecular dynamics simulation, cholesterol prevented the penetration of  $A\beta_{10-40}$  into the bilayer and it reduced thinning of the membrane below  $A\beta$ . These different results may be accounted for by the short time span of all-atom simulations.

Here, we perform molecular dynamics simulations using the coarse-grained Martini force field. This force field was parametrized to reproduce experimentally free energies of amino acid partition at the water-bilayer interface<sup>49</sup> and, thus, it is expected to provide an experimentally consistent description of how rigid protein conformations (e.g., amyloid fibrils) partition at the water-lipid interface. We compute fibril-bilayer binding probabilities for simulations performed using two different amyloid fibril structures with different surface charges and four bilayers with different lipid compositions. We find that electrostatic interactions play an important role in fibril-bilayer binding and cholesterol can modulate this interaction. In particular, the insertion of cholesterol into the bilayer leaves negatively charged moieties of lipid head groups more exposed on the surface where they can bind directly to charged residues of fibrils. This accounts for a net attractive force between the fibril and bilayer. Accordingly, we observe an increase in the number of fibril membrane binding events with an increasing cholesterol content of bilayers.

#### METHODOLOGY

Simulations are performed using the Martini 2.0 force field, <sup>49,50</sup> which models approximately every four heavy atoms of a lipid by one bead. Similarly, every four water molecules are represented by one solvent bead in this force field. Amino acids are described by two beads, which mimic the backbone and side chains of proteins. Parameters for the Martini model were originally determined using the potential of mean force for each amino acid as a function of distance from lipid bilayers. Partitioning of amino acids and lipid bilayers was also extensively used in the parameterization and

compared to atomistic simulations showing good agreement. <sup>49,50</sup> More recently, substantial modifications of the Martini water model were introduced in the POL-Martini and BMW-Martini <sup>52</sup> models to account for the polarizability and inner electrostatic structure of water. These models provide a better description of the transport of charged species between high- and low-dielectric mediums, as well as improved thermodynamic properties of water. The main strength of the original Martini water model is its speed as its description entails less points of interaction compared to the other water models while at the same time explicitly considering water molecules. This is a much better consideration than other coarse-grained models that only take implicit account of the solvent.

The Martini representation of the three lipids used in this study and the charge of their head group beads is shown in Figure 1b. Different symmetric bilayers made using these three lipids were prepared using the "insane" script. <sup>53</sup> In the following, we denote bilayers (i) entirely composed of dipalmitoylphosphatidylcholine (DPPC) lipids as PC, (ii) containing 30 and 50% cholesterol as CHOL<sub>30</sub> and CHOL<sub>50</sub>, respectively, and (iii) containing 10% diethylenetriaminepentaacetic acid (DTPA) lipids as PA. Sodium ions were added to neutralize the net charge of the system, and simulations were performed at physiological sodium chloride concentration, i.e., 0.15 M. Table S1 lists the number of lipids and water molecules for each system studied here.

For the atomic structure of  $A\beta$  fibrils, two ssNMR-derived fibril models, the  $A\beta_{17-42}$  2BEG<sup>54</sup> and the  $A\beta_{11-42}$  2MXU,<sup>55</sup> were used. To control for size differences between 2BEG and 2MXU conformations, the 5-peptide 2BEG fibril was modified to instead contain 12 replicated peptides to match the 12-peptide 2MXU fibril. Figure 1a shows the amino acid sequence of  $A\beta_{1-42}$ , as well as Martini representations of 2BEG and 2MXU fibrils formed with 12 peptides each. To maintain the fibril structure stable throughout the simulation, a global elastic network is used to connect peptide beads. Commonly used values for the elastic bond strength (500 kJ/(mol nm²)) and

upper bond cutoff (0.9 nm) of the elastic network are used. Molecular dynamics simulations are performed using the GROMACS suite version 5.2. Tequations of motion for each bead are solved using the leap-frog algorithm and a time step of 9.7 fs. The v-rescale thermostat ( $\tau_T = 0.1$  ps) and the semi-isotropic Parrinello–Rahman barostat ( $\tau_P = 0.1$  ps) are used to maintain the temperature and pressure constant at 345 K and 1 atm, respectively. A radius cutoff of 1.1 nm is used for van der Waals and electrostatic interactions. The latter are treated using the reaction field method. A schematic representation of our simulation setup is depicted in Figure 1c, where the minimal distance between the fibril and PO<sub>4</sub> beads of DPPC head groups is highlighted. This quantity is used as our estimate for the distance between the fibril and the surface of the membrane.

# RESULTS

The time dependence of the minimal fibril—membrane distance is shown in Figure 1d,e for simulations performed using 2BEG and 2MXU fibrils and the PC bilayer. Different levels of the proximity of the fibril to the membrane are seen in these 6  $\mu$ s trajectories. To gather enough statistics, four 6  $\mu$ s trajectories are produced for each system studied here with fibrils initialized at different positions in the simulation box. Histograms of minimal distances computed for the accumulated trajectories of these four simulations are shown in Figure 1f,g for the 2BEG and 2MXU fibrils and the PC bilayer. These histograms are characterized by a peak at distances smaller than 1 nm. This distance, i.e., 1 nm, is used as our cutoff to distinguish between bound and unbound states of the fibril—membrane system.

The time dependence of the minimal fibril-membrane distance for all of the systems studied here is shown in Section S2. The table in Figure 1h summarizes binding events from all of the simulations. The 2BEG fibril, which has mainly nonpolar residues exposed to the solvent, spends approximately 11% of the time bound to bilayers independently of their lipid composition. In contrast, the 2MXU fibril, which has several charged residues exposed to the solvent, is much more sensitive to lipid composition. Adding 30% cholesterol to a PC bilayer increases the number of binding events by a factor of 1.5 (from 13 to 20%). This effect of cholesterol is, however, not additive as enhancing its membrane content to 50% does not produce a further increase in fibril-membrane binding. The effect of adding DTPA lipids to the membrane is even more dramatic. In two out of the four simulations performed, the 2MXU fibril binds to the bilayer irreversibly after an induction time of a few microseconds. In these two simulations, 2MXU is bound to the membrane 55% of the time. One of these trajectories, which has an induction time of  $\sim$ 2.5  $\mu$ s, is shown in Figure 2a. In the other two simulations, the 2MXU fibril spends 14% of the time bound to the membrane (see Figure 2b for an example).

In summary, Figure 1h indicates that fibrils without surface charge bind minimally to bilayers independently of lipid composition. In contrast, fibrils that have charged residues on their surface can either modestly or markedly increase the amount of binding events. Strong binding is observed for bilayers containing lipids with negative head groups. This highlights the effects of charges on fibril—bilayer binding. Surprisingly, adding cholesterol (uncharged) to PC bilayers, which reduces the number of partial charges per unit

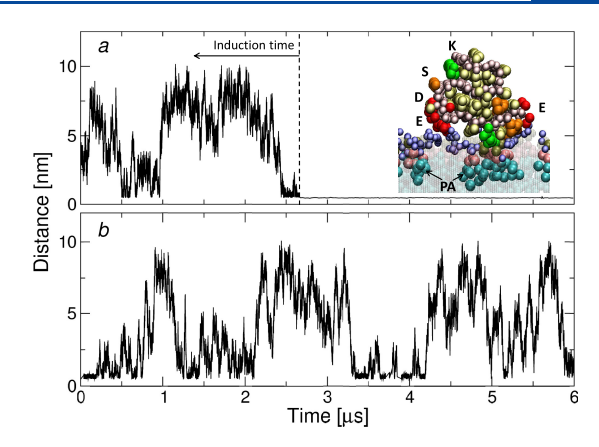


**Figure 2.** Minimal distances of 2MXU fibril and PA bilayers in two 6  $\mu$ s simulations. (a) Fibril binds irreversibly to the membrane after an induction time of ~2.5  $\mu$ s. A characteristic configuration is shown in the inset. (b) Several binding and unbinding events are observed.

membrane area, substantially increases the amount of binding events of the charged 2MXU fibril.

In Figure 3a, the distribution of binding events per amino acid type is shown for the different fibril-bilayer systems. We define a binding event to be of type X (where X can be nonpolar, polar, negative, positive, or other), if the shortest distance between the fibril and PO<sub>4</sub> beads occurs for an amino acid of type X. The main amino acids of 2MXU fibrils to bind to PC bilayers are negative E and D residues. Panel b depicts the two main binding configurations that are mediated by these negative residues and account for approximately 60% of all of the binding events. In these configurations, negative (red) and positive (green) residues are close to and far from positive NC<sub>3</sub> lipid beads, respectively. The addition of 30% cholesterol to PC bilayers does not significantly change the types of amino acids that bind to the membrane, and configurations in panel b remain the main binding modes of 2MXU fibrils. The addition of 50% cholesterol to PC bilayers accounts for a small increase in the number of polar binding events. A visual inspection of the trajectories for this system shows a significant increase in binding configurations, wherein positive residues are closer to NC<sub>3</sub> lipid beads. Panel c provides examples of such configurations, wherein positive and negative residues are in contact with the bilayer. A possible explanation for these effects of cholesterol is that it reduces the repulsion between positive residues and the membrane accounting for the observed increased binding in CHOL<sub>30</sub> bilayers. At high levels, i.e., CHOL50, positive residues may even become attracted to the membrane, leading to the different binding configurations observed in Figure 3c. Notice that polar residues (in orange) located between positive and negative amino acids can penetrate deep in the bilayer when these charged residues are simultaneously attracted to the membrane. This nontrivial effect on positive species by an uncharged lipid is further discussed in Figure 4.

In Figure 3a, the two simulations in which 2MXU binds irreversibly to PA bilayers are analyzed separately from the two simulations in which binding occurs reversibly. For the latter (referred to as PA), the distribution of binding events per amino acid is comparable to the one measured for PC bilayers: it is dominated by negative residues that can bind NC<sub>3</sub> beads exposed to the solvent. In the trajectories where binding occurs irreversibly (referred to as PA\*), binding is dominated by positive residues. An example of a binding conformation is

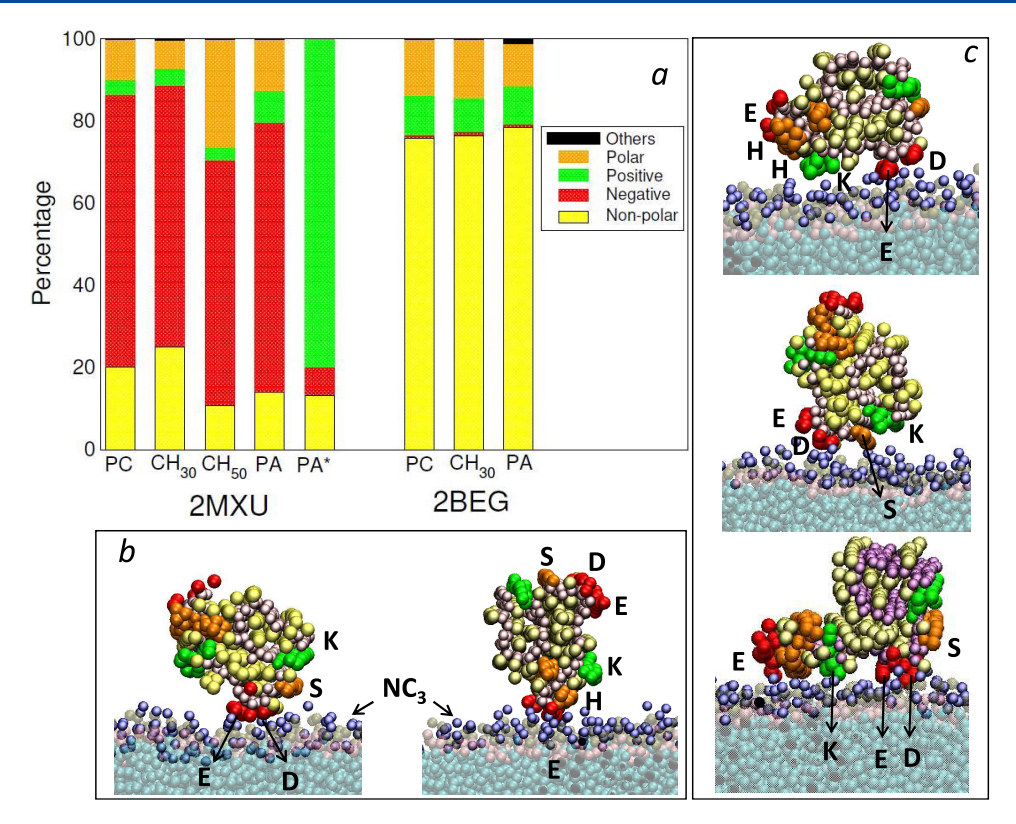


Figure 3. (a) Contributions of the residue type to 2BEG and 2MXU bindings to lipid bilayers. Residues are nonpolar (A, V, I, L, F, and M), negative (E and D), positive (K), and polar (S, H, and N). The main binding conformations are shown for the (b) PC and CHOL $_{30}$  and (c) CHOL $_{50}$  2MXU-bilayer systems. Bilayers containing DTPA lipids in which binding occurs reversibly and irreversibly are labeled PA and PA\*, respectively.

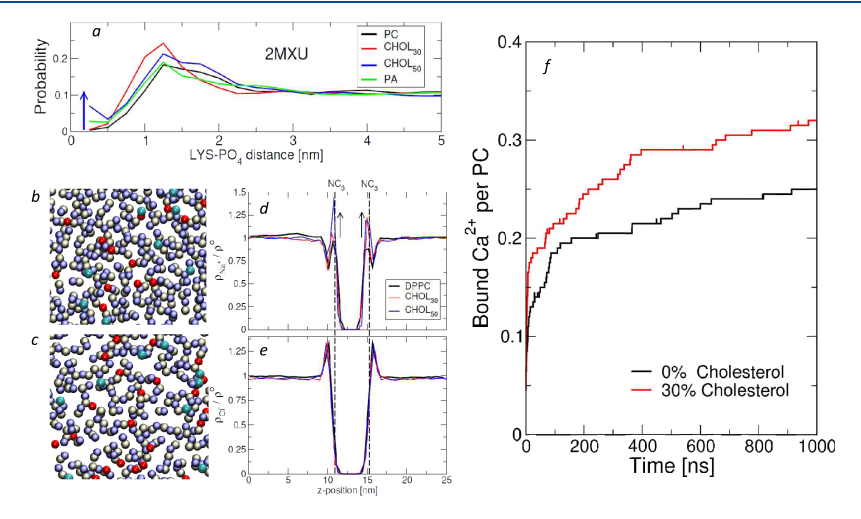


Figure 4. (a) Probability distribution of the distance between lysine and  $PO_4$  beads for different bilayers. Characteristic membrane-ion conformations for (b) PC and (c) CHOL<sub>50</sub> bilayers. Red and cyan spheres represent Na<sup>+</sup> and CL<sup>-</sup> ions, respectively, whereas purple and beige spheres correspond to NC<sub>3</sub> and PO<sub>4</sub> beads of DPPC lipids. In these particular conformations, there are (b) 13 Na<sup>+</sup> and 8 CL<sup>-</sup> and (c) 22 Na<sup>+</sup> and 9 Cl<sup>-</sup> ions. Normalized densities of (d) Na<sup>+</sup> and (e) CL<sup>-</sup> as a function of the distance from the bilayer center. (f) Number of Ca<sup>2+</sup> ions bound to PC lipids in all-atom simulations containing 0 and 30% cholesterol.

shown in the inset of Figure 2a, wherein lysine binds to negative PO<sub>4</sub> bead of DTPA head groups. Assuming that binding events in PA simulations are representative of events occurring during the induction time of PA\* (see Figure 2), these results suggest that negative residues of 2MXU fibrils bind first to exposed positive NC<sub>3</sub> beads followed by binding of the positive lysine residues to PO<sub>4</sub> beads of PA lipids. Figure 3a also shows the distributions of binding events for the 2BEG

fibril. Consistent with the results listed in Figure 1h, the amino acid distributions of binding events do not change significantly with the bilayer composition. In addition, 70% of binding events occur between nonpolar residues and the bilayer, consistent with the predominantly nonpolar surface of the fibril exposed to the solvent.

To provide insights into how cholesterol affects the binding of positive amino acids to bilayers, we show in Figure 4a the probability distribution of the minimum distance  $d_{LYS}$  between lysine residues of 2MXU fibrils and negative PO<sub>4</sub> beads of DPPC lipids. Small values of  $d_{LYS}$  ( $\leq 0.5$  nm) are not found in simulations performed with PC (black line) and CHOL<sub>30</sub> (red) bilayers, implying the absence of a direct contact between lysine and PO<sub>4</sub> beads. Moreover, the high percentage of binding events in CHOL<sub>30</sub> simulations (see Figure 1h) accounts for the proximity of lysine residues to bilayers, which is characterized by the more pronounced peak at  $d_{\rm LYS} \sim 1$  nm. For PA and CHOL50 bilayers, several configurations are characterized by  $d_{LYS}$  values smaller than 0.5 nm, providing evidence that lysine and PO<sub>4</sub> beads are attracted to each other. This is highlighted by the blue arrow in Figure 4a. In summary, Figure 4a shows that lysine is found closer to the membrane in CHOL<sub>30</sub> than in PC bilayers. Moreover, this positive residue is attracted to PO<sub>4</sub> beads in CHOL<sub>50</sub> bilayers.

Insights on how an uncharged lipid can favor the interaction between positive lysine and zwitterionic bilayers can be obtained by studying cations. Multivalent and some monovalent cations in aqueous solution have been shown to penetrate the positive NC<sub>3</sub> layer to interact with negative phosphate moieties of lipid head groups.<sup>58</sup> To study the effects of cholesterol on cations within the Martini force field, we show in Figure 4b,c the characteristic spatial distributions of Na<sup>+</sup> and Cl<sup>-</sup> in PC and CHOL<sub>50</sub> bilayers, respectively. Notice that other ions have not been parametrized for the Martini force field. In these figures, most Na<sup>+</sup> ions are located deep within the bilayer where they interact with negative PO<sub>4</sub> beads. In Figure S3, we show that cholesterol increases the area per DPPC head groups.<sup>59</sup> This enables Na<sup>+</sup> to more easily penetrate into the NC<sub>3</sub> layer to interact with PO<sub>4</sub> beads. Accordingly, a larger number of Na+ ions can be seen at the bilayer surface in panel c compared to those in panel b. This is shown quantitatively in panel d, wherein increasing the cholesterol content increases the relative density of Na+ close to the bilayer. Panel e shows that cholesterol has no significant effect on the distribution of Cl- ions. These effects of cholesterol on the binding of ions to lipid bilayers are not limited to the Martini force field and they are also observed in all-atom simulations. Figure 4f shows results from two all-atom simulations using the CHARMM36 force field and TIP3P water. In these simulations, the bilayer is made of 200 POPC lipids and the solution contains 450 mM of CaCl<sub>2</sub>. In one of the simulations, the bilayer also contains 86 cholesterol molecules, which accounts for 30% of the lipid content. The number of Ca<sup>2+</sup> ions bound to PC lipids is shown in this figure as a function of time for our two simulations. This number is computed using a 0.325 nm distance cutoff between oxygen atoms of phosphate moieties of POPC and Ca<sup>2+,59</sup> The number of bound calcium ions is higher in bilayers containing cholesterol which is consistent with our results using the Martini force field. Recent all-atom simulations have shown that this effect of cholesterol is observed for different force fields.59

Assuming that the effects of cholesterol on positive and negative residues are similar to its effects on cations and anions, respectively, we can extrapolate these ion results to 2MXU-bilayer binding. It implies that the addition of cholesterol to bilayers does not increase the binding of negative residues, whereas it reduces the repulsion of positive residues from the membrane. The latter interaction may even become favorable at high cholesterol concentrations. These results are consistent with the observed enhancement of

2MXU-bilayer binding with increased cholesterol concentrations, the characteristic binding conformations in Figure 3c, and  $d_{\rm LYS}$  distributions in Figure 4a.

# CONCLUSIONS

In conclusion, our simulations show that electrostatic interactions between charges on fibrils and bilayer are important in determining binding and specific contacts between these species. More importantly, our results show that adding cholesterol (uncharged) to the bilayer increases the binding frequency and modulates the nature of contacts. This role of cholesterol is rationalized in terms of its effect on the interaction between positive residues and lipid head groups. Despite these novel insights, it is also important to highlight limitations of the current work. In particular, the original Martini water model used in this work does not provide screening for electrostatic interactions. Thus, the binding frequency of charged species, i.e., ions and charged residues, to partially charged moieties of lipids might be overestimated. However, the qualitative role of cholesterol reported here is expected to remain valid in simulations using more realistic force fields as this sterol enhances the exposure of charged moieties of lipid molecules to the solvent. This is supported by all-atom simulations in which cholesterol was shown to enhance Ca<sup>++</sup>-bilayer binding.<sup>59</sup>

# ASSOCIATED CONTENT

### Supporting Information

The Supporting Information is available free of charge at https://pubs.acs.org/doi/10.1021/acs.jpcb.0c00485.

(1) Description of all simulations performed in the work; (2) minimal fibril—bilayer distance for all simulations; (3) effects of cholesterol on a bilayer made of DPPC lipids (PDF)

#### AUTHOR INFORMATION

# **Corresponding Author**

Cristiano L. Dias — Department of Physics, New Jersey Institute of Technology, Newark, New Jersey 07102-1982, United States; occid.org/0000-0002-8765-3922; Email: cld@njit.edu

#### **Authors**

Sharareh Jalali – Department of Physics, New Jersey Institute of Technology, Newark, New Jersey 07102-1982, United States
Yanxing Yang – Department of Physics, New Jersey Institute of Technology, Newark, New Jersey 07102-1982, United States
Luis Cruz – Department of Physics, Drexel University, Philadelphia, Pennsylvania 19104, United States

Complete contact information is available at: https://pubs.acs.org/10.1021/acs.jpcb.0c00485

#### Notes

The authors declare no competing financial interest.

# ACKNOWLEDGMENTS

This material is based upon the work supported by the National Science Foundation under Grant Nos. CHE-1904364 and CHE-1904528. Computational resources were provided by the High Performance Computing Center at the New Jersey Institute of Technology.

#### REFERENCES

- (1) Stefani, M.; Dobson, C. M. Protein aggregation and aggregate toxicity: new insights into protein folding, misfolding diseases and biological evolution. *J. Mol. Med.* **2003**, *81*, 678–699.
- (2) Chiti, F.; Dobson, C. M. Protein misfolding, functional amyloid, and human disease. *Annu. Rev. Biochem.* **2006**, *75*, 333–366.
- (3) Owen, M. C.; Gnutt, D.; Gao, M.; Wärmländer, S. K.; Jarvet, J.; Gräslund, A.; Winter, R.; Ebbinghaus, S.; Strodel, B. Effects of in vivo conditions on amyloid aggregation. *Chem. Soc. Rev.* **2019**, *48*, 3946–3996.
- (4) Kotler, S. A.; Walsh, P.; Brender, J. R.; Ramamoorthy, A. Differences between amyloid-beta aggregation in solution and on the membrane: insights into elucidation of the mechanistic details of Alzheimer's disease. *Chem. Soc. Rev.* **2014**, *43*, 6692–6700.
- (5) Haass, C.; Selkoe, D. J. Soluble protein oligomers in neurodegeneration: lessons from the Alzheimer's amyloid  $\beta$ -peptide. *Nat. Rev. Mol. Cell Biol.* **2007**, *8*, 101–112.
- (6) Milanesi, L.; Sheynis, T.; Xue, W. F.; Orlova, E. V.; Hellewell, A. L.; Jelinek, R.; Hewitt, E. W.; Radford, S. E.; Saibil, H. R. Direct three-dimensional visualization of membrane disruption by amyloid fibrils. *Proc. Natl. Acad. Sci. U.S.A.* **2012**, *109*, 20455–20460.
- (7) Engel, M. F. M.; Khemtemourian, L.; Kleijer, C. C.; Meeldijk, H. J. D.; Jacobs, J.; Verkleij, A. J.; de Kruijff, B.; Killian, J. A.; Hoppener, J. W. M. Membrane damage by human islet amyloid polypeptide through fibril growth at the membrane. *Proc. Natl. Acad. Sci. U.S.A.* **2008**, *105*, 6033–6038.
- (8) Tipping, K. W.; van Oosten-Hawle, P.; Hewitt, E. W.; Radford, S. E. Amyloid fibres: inert end-stage aggregates or key players in disease. *Trends Biochem. Sci.* **2015**, *40*, 719–727.
- (9) Straub, J. E.; Thirumalai, D. Membrane-protein interactions are key to understanding amyloid formation. *J. Phys. Chem. Lett.* **2014**, *5*, 633–635.
- (10) Zhang, X.; St. Clair, J. R.; London, E.; Raleigh, D. P. Islet amyloid polypeptide membrane interactions: effects of membrane composition. *Biochemistry* **2017**, *56*, 376–390.
- (11) Drolle, E.; Negoda, A.; Hammond, K.; Pavlov, E.; Leonenko, Z. Changes in lipid membranes may trigger amyloid toxicity in Alzheimer's disease. *PLOS One* **2017**, *12*, No. e0182194.
- (12) Bucciantini, M.; Rigacci, S.; Stefani, M. Amyloid aggregation: Role of biological membranes and the aggregate-membrane system. *J. Phys. Chem. Lett.* **2014**, *5*, 517–527.
- (13) Stefani, M.; Liguri, G. Cholesterol in Alzheimer's disease: unresolved questions. *Curr. Alzheimer Res.* **2009**, *6*, 15–29.
- (14) Tashima, Y.; Oe, R.; Lee, S.; Sugihara, G.; Chambers, E. J.; Takahashi, M.; Yamada, T. The effect of cholesterol and monosialoganglioside (GM1) on the release and aggregation of amyloid  $\beta$ -peptide from liposomes prepared from brain membrane-like lipids. *J. Biol. Chem.* **2004**, *279*, 17587–17595.
- (15) Di Paolo, G.; Kim, T.-W. Linking lipids to Alzheimer's disease: cholesterol and beyond. *Nat. Rev. Neurosci.* 2011, 12, 284–296.
- (16) Matsuzaki, T.; Sasaki, K.; Hata, J.; Hirakawa, Y.; Fujimi, K.; Ninomiya, T.; Suzuki, S.; Kanba, S.; Kiyohara, Y.; Iwaki, T. Association of Alzheimer disease pathology with abnormal lipid metabolism: the Hisayama study. *Neurology* **2011**, *77*, 1068–1075.
- (17) Pappolla, M. A.; Bryant-Thomas, T.; Herbert, D.; Pacheco, J.; Garcia, M. F.; Manjon, M.; Girones, X.; Henry, T.; Matsubara, E.; Zambon, D.; et al. Mild hypercholesterolemia is an early risk factor for the development of Alzheimer amyloid pathology. *Neurology* **2003**, *61*, 199–205.
- (18) Maulik, M.; Westaway, D.; Jhamandas, J.; Kar, S. Role of cholesterol in APP metabolism and its significance in Alzheimer's disease pathogenesis. *Mol. Neurobiol.* **2013**, 47, 37–63.
- (19) Ingólfsson, H. I.; Carpenter, T. S.; Bhatia, H.; Bremer, P.-T.; Marrink, S. J.; Lightstone, F. C. Computational lipidomics of the neuronal plasma membrane. *Biophys. J.* **2017**, *113*, 2271–2280.
- (20) DelBove, C. E.; Strothman, C. E.; Lazarenko, R. M.; Huang, H.; Sanders, C. R.; Zhang, Q. Reciprocal modulation between amyloid precursor protein and synaptic membrane cholesterol revealed by live cell imaging. *Neurobiol. Dis.* **2019**, *127*, 449–461.

- (21) von Arnim, C. A. F.; von Einem, B.; Weber, P.; Wagner, M.; Schwanzar, D.; Spoelgen, R.; Strauss, W. L.; Schneckenburger, H. Impact of cholesterol level upon APP and BACE proximity and APP cleavage. *Biochem. Biophys. Res. Commun.* **2008**, 370, 207–212.
- (22) Xiong, H.; Callaghan, D.; Jones, A.; Walker, D. G.; Lue, L.-F.; Beach, T. G.; Sue, L. I.; Woulfe, J.; Xu, H.; Stanimirovic, D. B.; et al. Cholesterol retention in Alzheimer's brain is responsible for high  $\beta$ -and  $\gamma$ -secretase activities and  $A\beta$  production. *Neurobiol. Dis.* **2008**, 29, 422–437.
- (23) Wood, W. G.; Li, L.; Muller, W. E.; Eckert, G. P. Cholesterol as a causative factor in Alzheimer's disease: a debatable hypothesis. *J. Neurochem.* **2014**, *129*, 559–572.
- (24) Habchi, J.; Chia, S.; Galvagnion, C.; Michaels, T. C. T.; Bellaiche, M. M. J.; Ruggeri, F. S.; Sanguanini, M.; Idini, I.; Kumita, J. R.; Sparr, E.; et al. Cholesterol catalyses  $A\beta_{42}$  aggregation through a heterogeneous nucleation pathway in the presence of lipid membranes. *Nat. Chem.* **2018**, *10*, 673–683.
- (25) Drolle, E.; Gaikwad, R. M.; Leonenko, Z. Nanoscale electrostatic domains in cholesterol-laden lipid membranes create a target for amyloid binding. *Biophys. J.* **2012**, *103*, L27–L29.
- (26) Ji, S.-R.; Wu, Y.; Sui, S.-f. Cholesterol is an important factor affecting the membrane insertion of beta-amyloid peptide ( $A\beta_{1-40}$ ), which may potentially inhibit the fibril formation. *J. Biol. Chem.* **2002**, 277, 6273–6279.
- (27) Bharadwaj, P.; Solomon, T.; Malajczuk, C. J.; Mancera, R. L.; Howard, M.; Arrigan, D. W.; Newsholme, P.; Martins, R. N. Role of the cell membrane interface in modulating production and uptake of Alzheimer's beta amyloid protein. *Biochim. Biophys. Acta, Biomembr.* **2018**, *1860*, 1639–1651.
- (28) Butterfield, S. M.; Lashuel, H. A. Amyloidogenic protein-membrane interactions: mechanistic insight from model systems. *Angew. Chem., Int. Ed.* **2010**, *49*, 5628–5654.
- (29) Kollmer, M.; Meinhardt, K.; Haupt, C.; Liberta, F.; Wulff, M.; Linder, J.; Handl, L.; Heinrich, L.; Loos, C.; Schmidt, M.; et al. Electron tomography reveals the fibril structure and lipid interactions in amyloid deposits. *Proc. Natl. Acad. Sci. U.S.A.* **2016**, *113*, 5604–5609.
- (30) Han, S.; Kollmer, M.; Markx, D.; Claus, S.; Walther, P.; Fändrich, M. Amyloid plaque structure and cell surface interactions of  $\beta$ -amyloid fibrils revealed by electron tomography. *Sci. Rep.* **2017**, 7, No. 43577.
- (31) Reynolds, N. P.; Soragni, A.; Rabe, M.; Verdes, D.; Liverani, E.; Handschin, S.; Riek, R.; Seeger, S. Mechanism of membrane interaction and disruption by  $\alpha$ -synuclein. *J. Am. Chem. Soc.* **2011**, 133, 19366–19375.
- (32) Grudzielanek, S.; Smirnovas, V.; Winter, R. The effects of various membrane physical-chemical properties on the aggregation kinetics of insulin. *Chem. Phys. Lipids* **2007**, *149*, 28–39.
- (33) Xue, W.-F.; Hellewell, A. L.; Gosal, W. S.; Homans, S. W.; Hewitt, E. W.; Radford, S. E. Fibril fragmentation enhances amyloid cytotoxicity. *J. Biol. Chem.* **2009**, *284*, 34272–34282.
- (34) Sugiura, Y.; Ikeda, K.; Nakano, M. High membrane curvature enhances binding, conformational changes, and fibrillation of amyloid- $\beta$  on lipid bilayer surfaces. *Langmuir* **2015**, *31*, 11549–11557.
- (35) Chi, E. Y.; Ege, C.; Winans, A.; Majewski, J.; Wu, G.; Kjaer, K.; Lee, K. Y. C. Lipid membrane templates the ordering and induces the fibrillogenesis of Alzheimeras disease amyloid- $\beta$  peptide. *Proteins: Struct., Funct., Bioinf.* **2008**, 72, 1–24.
- (36) Hertel, C.; Terzi, E.; Hauser, N.; Jakob-Røtne, R.; Seelig, J.; Kemp, J. Inhibition of the electrostatic interaction between  $\beta$ -amyloid peptide and membranes prevents  $\beta$ -amyloid-induced toxicity. *Proc. Natl. Acad. Sci. U.S.A.* **1997**, *94*, 9412–9416.
- (37) Zhao, H.; Tuominen, E. K.; Kinnunen, P. K. Formation of amyloid fibers triggered by phosphatidylserine-containing membranes. *Biochemistry* **2004**, *43*, 10302–10307.
- (38) Pannuzzo, M.; Raudino, A.; Milardi, D.; La Rosa, C.; Karttunen, M.  $\alpha$ -Helical structures drive early stages of self-assembly

- of amyloidogenic amyloid polypeptide aggregate formation in membranes. Sci. Rep. 2013, 3, No. 2781.
- (39) Pannuzzo, M. On the physiological/pathological link between  $A\beta$  peptide, cholesterol, calcium ions and membrane deformation: A molecular dynamics study. *Biochim. Biophys. Acta, Biomembr.* **2016**, 1858, 1380–1389.
- (40) Di Scala, C.; Chahinian, H.; Yahi, N.; Garmy, N.; Fantini, J. Interaction of Alzheimeras  $\beta$ -amyloid peptides with cholesterol: mechanistic insights into amyloid pore formation. *Biochemistry* **2014**, 53, 4489–4502.
- (41) Seghezza, S.; Diaspro, A.; Canale, C.; Dante, S. Cholesterol drives  $A\beta$  (1–42) interaction with lipid rafts in model membranes. *Langmuir* **2014**, *30*, 13934–13941.
- (42) Sodt, A. J.; Sandar, M. L.; Gawrisch, K.; Pastor, R. W.; Lyman, E. The molecular structure of the liquid-ordered phase of lipid bilayers. *J. Am. Chem. Soc.* **2014**, *136*, 725–732.
- (43) Radovan, D.; Opitz, N.; Winter, R. Fluorescence microscopy studies on islet amyloid polypeptide fibrillation at heterogeneous and cellular membrane interfaces and its inhibition by resveratrol. *FEBS Lett.* **2009**, 583, 1439–1445.
- (44) Tofoleanu, F.; Brooks, B. R.; Buchete, N. V. Modulation of Alzheimeras  $A\beta$  protofilament-membrane interactions by lipid headgroups. *ACS Chem. Neurosci.* **2015**, *6*, 446–455.
- (45) Yu, X.; Zheng, J. Cholesterol promotes the interaction of Alzheimer beta-amyloid monomer with lipid bilayer. *J. Mol. Biol.* **2012**, *421*, 561–571.
- (46) Jang, H.; Connelly, L.; Teran Arce, F.; Ramachandran, S.; Kagan, B. L.; Lal, R.; Nussinov, R. Mechanisms for the insertion of toxic, fibril-like  $\beta$ -amyloid oligomers into the membrane. *J. Chem. Theory Comput.* **2013**, *9*, 822–833.
- (47) Yu, X.; Wang, Q.; Pan, Q.; Zhou, F.; Zheng, J. Molecular interactions of Alzheimer amyloid-β oligomers with neutral and negatively charged lipid bilayers. *Phys. Chem. Chem. Phys.* **2013**, *15*, 8878–8889.
- (48) Lockhart, C.; Klimov, D. K. Cholesterol changes the mechanisms of  $A\beta$  peptide binding to the DMPC bilayer. *J. Chem. Inf. Model.* **2017**, *57*, 2554–2565.
- (49) Monticelli, L.; Kandasamy, S. K.; Periole, X.; Larson, R. G.; Tieleman, D. P.; Marrink, S.-J. The MARTINI coarse-grained force field: extension to proteins. *J. Chem. Theory Comput.* **2008**, *4*, 819–834.
- (50) Marrink, S. J.; Risselada, H. J.; Yefimov, S.; Tieleman, D. P.; De Vries, A. H. The MARTINI force field: coarse grained model for biomolecular simulations. *J. Phys. Chem. B* **2007**, *111*, 7812–7824.
- (51) Yesylevskyy, S. O.; Schäfer, L. V.; Sengupta, D.; Marrink, S. J. Polarizable water model for the coarse-grained MARTINI force field. *PLOS Comput. Biol.* **2010**, *6*, No. e1000810.
- (52) Wu, Z.; Cui, Q.; Yethiraj, A. A new coarse-grained force field for membrane-peptide simulations. *J. Chem. Theory Comput.* **2011**, 7, 3793–3802.
- (53) Wassenaar, T. A.; Ingólfsson, H. I.; Bockmann, R. A.; Tieleman, D. P.; Marrink, S. J. Computational lipidomics with insane: a versatile tool for generating custom membranes for molecular simulations. *J. Chem. Theory Comput.* **2015**, *11*, 2144–2155.
- (54) Luhrs, T.; Ritter, C.; Adrian, M.; Riek-Loher, D.; Bohrmann, B.; Dobeli, H.; Schubert, D.; Riek, R. 3D structure of Alzheimer's amyloid-beta(1-42) fibrils. *Proc. Natl. Acad. Sci. U.S.A.* **2005**, *102*, 17342–17347.
- (55) Xiao, Y. L.; Ma, B. Y.; McElheny, D.; Parthasarathy, S.; Long, F.; Hoshi, M.; Nussinov, R.; Ishii, Y. A beta(1-42) fibril structure illuminates self-recognition and replication of amyloid in Alzheimer's disease. *Nat. Struct. Mol. Biol.* **2015**, 22, 499–U97.
- (56) Periole, X.; Cavalli, M.; Marrink, S.-J.; Ceruso, M. A. Combining an elastic network with a coarse-grained molecular force field: structure, dynamics, and intermolecular recognition. *J. Chem. Theory Comput.* **2009**, *5*, 2531–2543.
- (57) Abraham, M. J.; Murtola, T.; Schulz, R.; Páll, S.; Smith, J. C.; Hess, B.; Lindahl, E. GROMACS: High performance molecular

- simulations through multi-level parallelism from laptops to supercomputers. *SoftwareX* **2015**, *1*–2, 19–25.
- (58) Catte, A.; Girych, M.; Javanainen, M.; Loison, C.; Melcr, J.; Miettinen, M. S.; Monticelli, L.; Määttä, J.; Oganesyan, V. S.; Ollila, O. S.; et al. Molecular electrometer and binding of cations to phospholipid bilayers. *Phys. Chem. Chem. Phys.* **2016**, *18*, 32560–32569
- (59) Javanainen, M.; Melcrová, A.; Magarkar, A.; Jurkiewicz, P.; Hof, M.; Jungwirth, P.; Martinez-Seara, H. Two cations, two mechanisms: interactions of sodium and calcium with zwitterionic lipid membranes. *Chem. Commun.* **2017**, *53*, 5380–5383.